

HeLiPR: Heterogeneous LiDAR Dataset for inter-LiDAR Place Recognition under Spatial and Temporal Variations

Journal Title
XX(X):i-ix
©The Author(s) 2023
Reprints and permission:
sagepub.co.uk/journalsPermissions.nav
DOI: 10.1177/ToBeAssigned
www.sagepub.com/

SAGE

Minwoo Jung¹, Wooseong Yang¹, Dongjae Lee¹, Hyeonjae Gil¹, Giseop Kim², Ayoung Kim¹

Abstract

Place recognition is crucial for robotic localization and loop closure in simultaneous localization and mapping (SLAM). Recently, LiDARs have gained popularity due to their robust sensing capability and measurement consistency, even in the illumination-variant environment, offering an advantage over traditional imaging sensors. Spinning LiDARs are widely accepted among many types, while non-repetitive scanning patterns have recently been utilized in robotic applications. Beyond the range measurements, some LiDARs offer additional measurements, such as reflectivity, Near Infrared (NIR), and velocity (e.g., FMCW LiDARs). Despite these advancements, a noticeable dearth of datasets comprehensively reflects the broad spectrum of LiDAR configurations optimized for place recognition. To tackle this issue, our paper proposes the HeLiPR dataset, curated especially for place recognition with heterogeneous LiDAR systems, embodying spatial-temporal variations. To the best of our knowledge, the HeLiPR dataset is the first heterogeneous LiDAR dataset designed to support inter-LiDAR place recognition with both non-repetitive and spinning LiDARs, accommodating different field of view (FOV) and varying numbers of rays. Encompassing the distinct LiDAR configurations, it captures varied environments ranging from urban cityscapes to high-dynamic freeways over a month, designed to enhance the adaptability and robustness of place recognition across diverse scenarios. Notably, the HeLiPR dataset also includes trajectories that parallel sequences from MulRan, underscoring its utility for research in heterogeneous LiDAR place recognition and long-term studies. The dataset is accessible at <https://sites.google.com/view/heliprdataset>.

Keywords

Dataset, Multiple LiDARs, Heterogeneous LiDARs, Place Recognition, SLAM

1 Introduction

Place recognition is a crucial task in robotics, involving the ability to identify whether a place has been visited before or not. The significance of this task stems from its role as an initial step towards localization and its contribution to enabling loop closure in SLAM. Traditionally, it has been accomplished by conducting a query image search within a database using an image sensors (Zhang et al. 2010; Arandjelovic et al. 2016; Lee and Kim 2021). However, recent advancements have facilitated the adoption of Light Detection and Ranging (LiDAR) for place recognition, attributable to its exceptional sensing capabilities. LiDAR-based place recognition has been gaining attraction thanks to its capacity to measure the range precisely, and distinct from image sensors, LiDAR has the advantage of capturing geometric structures with illumination invariance, positioning it as an attractive alternative. Conventionally, LiDAR descriptors (Kim et al. 2021; Xu et al. 2022b; Luo et al. 2021) are generated from scan and subsequently used to ascertain the presence or absence of a place through comparison with a comprehensive set of descriptors.

With the advancement of place recognition, the hardware capabilities of LiDAR have also evolved significantly. For instance, specific LiDAR devices deploy non-repetitive scanning patterns to achieve dense mapping, thus deviating from traditional spinning LiDARs. Additionally, some LiDARs feature a more significant number of rays,

surpassing the conventional 16 or 32-ray configurations, and incorporate additional channels such as reflectivity and NIR. More recently, the advent of FMCW LiDAR has made it possible to measure relative velocity along the radial direction utilizing the doppler effect, commonly called velocity measurement. Considering this development in LiDARs, place recognition with non-repetitive scanning pattern LiDARs (Yuan et al. 2023) has also been pursued. Furthermore, studies (Wang et al. 2020; Shan et al. 2021; Chen et al. 2020) that leverage the information offered by the additional channels in LiDAR have also emerged.

Nevertheless, despite these advancements, there currently exists a scarcity of datasets incorporating diverse combinations of LiDARs for place recognition. This shortfall highlights a gap in the availability of benchmark datasets for evaluating and comparing place recognition operating with heterogeneous LiDARs. Several datasets (Kim et al. 2020; Knights et al. 2023; Geiger et al. 2012) are conducive for tasks involving place recognition, although they are equipped solely with a spinning LiDAR. On the other hand,

¹Dept. of Mechanical Engineering, SNU, Seoul, S. Korea

²NAVER LABS, Gyeonggi-do, S. Korea

Corresponding author:

Ayoung Kim, Dept. of Mechanical Engineering, SNU, Seoul, S. Korea
Email: ayoungk@snu.ac.kr

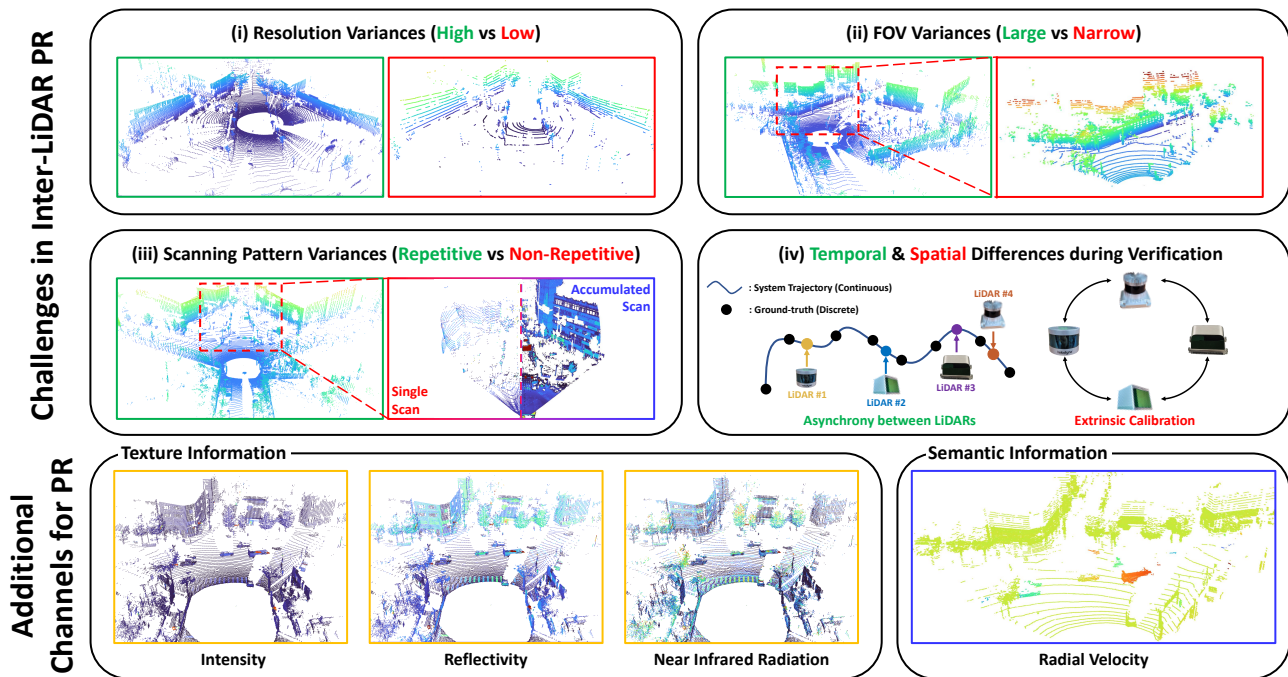


Figure 1. (Top row) LiDAR place recognition challenges (i) Variance in resolution between high and low ray count LiDARs affects sensing abilities. (ii) While some LiDARs perform full 360-degree scans, others have limited FOV due to occlusion or sensor limitations. (iii) Most LiDARs scan the same area, whereas non-repetitive LiDAR densely scan by stacking individual scans. However, each scan tends to be sparse, as depicted in the left red box. (iv) Ground truth, crucial for executing LiDAR place recognition, is challenging to determine due to varying LiDAR coordinates and scan acquisition times. (Bottom row) HeLiPR dataset provides heterogeneous LiDARs and additional channels, thereby granting opportunities to utilize texture information from LiDAR.

while there are datasets inclusive of multiple LiDARs, these predominantly feature spinning LiDARs (Jeong et al. 2019; Barnes et al. 2020; Agarwal et al. 2020; Hsu et al. 2021), or they comprise heterogeneous LiDARs that are ill-suited for place recognition (Qingqing et al. 2022; Helmberger et al. 2022; Jung et al. 2023).

This paper introduces the HeLiPR dataset, a unique heterogeneous LiDAR dataset for place recognition, encapsulating spatial and temporal variations. Regarding environmental diversity, our dataset spans a monthly duration, providing a variety of environments encompassing a narrow residential area, urban cityscape, and environments with high dynamic change. Furthermore, the HeLiPR dataset includes trajectories similar to sequences acquired from MulRan (Kim et al. 2020), enabling another heterogeneous LiDAR and long-term place recognition with a term of four years. The salient contributions of the HeLiPR dataset are as follows:

1. The HeLiPR dataset includes heterogeneous LiDARs, with OS2-128, VLP-16, Livox Avia, and Aeries II, while most of the existing dataset involves only spinning LiDARs. This configuration can underscore the impact of disparities in resolution and scanning patterns. Furthermore, their channels, such as NIR, reflectivity, and radial velocity, pave the way for novel strategies in place recognition.
2. The HeLiPR dataset tackles heterogeneous LiDAR place recognition. Based on our benchmark results, the HeLiPR dataset emphasizes the urgent need for dedicated research in heterogeneous inter-LiDAR place recognition. Furthermore, it accentuates the critical position of this dataset in catalyzing and guiding these essential explorations.

3. The HeLiPR dataset captures diverse environments monthly, from residential to dynamic urban areas. Furthermore, with trajectories akin to those in MulRan, it enables heterogeneous LiDAR place recognition and supports long-term research spanning four years. This broad spectrum of data acquisition positions HeLiPR as a pivotal tool for generalizing place recognition across varied scenarios.
4. The HeLiPR dataset provides individual LiDAR ground truth corresponding to the acquisition time of each LiDAR. This accurate ground truth, which also considers spatial relationships, facilitates more accessible validation and improves the reliability of place recognition.

2 Related works

This section presents an overview of LiDAR datasets pertinent to our research. A summary is provided in Table. 1.

The KITTI dataset (Geiger et al. 2012), gathered using a carlike vehicle, is representative of a mid-sized cityscape. While it facilitates intra-session place recognition, the dataset falls short in supporting inter-session place recognition, with data acquisition solely reliant on a single HDL-64E. On the other hand, the Oxford Robotcar Radar Dataset (Barnes et al. 2020), which shares a similar environment with KITTI, introduces the possibility for inter-session place recognition. However, even though multiple LiDARs are incorporated, all are of the spinning type. Another dataset, the Ford Multi-AV Dataset (Agarwal et al. 2020), which stands out due to its extensive trajectory covering a range of environments from urban to vegetated, including tunnels, and showcasing seasonal

Table 1. Dataset comparison for place recognition study. The * count represents added channels, inter-session diversity enabling place recognition in more diverse environments, and sequence length; more stars indicate a greater extent of these factors.

Datasets		KITTI	Complex Urban	Oxford Radar	Ford Multi AV	MulRan	NTU VIRAL	Boreas	Pohang Canal	Wild Place	Hilti	Tiers	HeLiPR
LiDAR	# Spinning	1	2	2	4	1	2	1	3	1	1	3	2
	# Solid State	X	X	X	X	X	X	X	X	X	1	3	2
	Additional Channels	X	X	X	X	X	**	X	**	X	**	**	***
Loop	Intra-session	✓	✓	✓	✓	✓	X	✓	X	✓	X	X	✓
	Inter-session	X	✓	✓	✓	✓	X	✓	✓	✓	X	X	✓
	Temporal Diversity	X	✓	X	✓	✓	X	✓	✓	✓	X	X	✓
	Inter-session Difference	X	*	X	X	**	X	X	X	*	X	X	***
Spatial Scale of Sequence		**	***	***	***	***	*	***	**	**	*	*	***
Total Distance		44km	190km	280km	198km	123km	1.9km	350km	45km	33km	2.1km	2km	145km

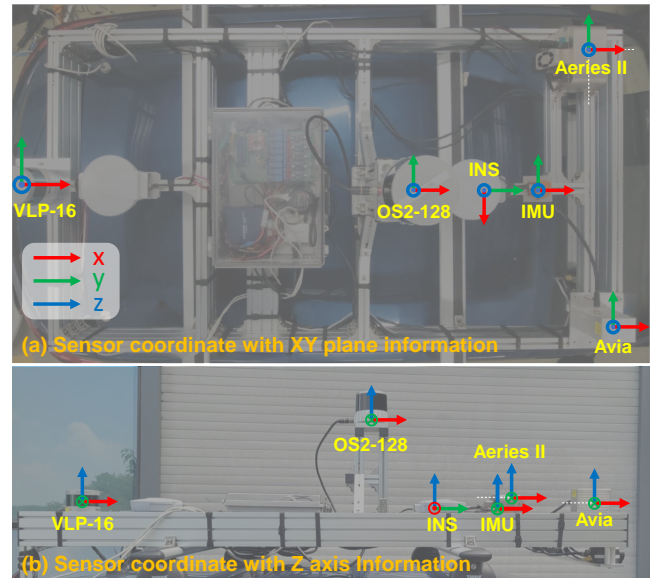
Table 2. The heterogeneous LiDARs utilized in Our Dataset

Sensor	Manufacture	Model	Channel	FOV (H×V)	Range
Spinning	Ouster	OS2-128	128	360° × 22.5°	200m
Spinning	Velodyne	VLP-16	16	360° × 30°	100m
Solid state	Livox	Avia	6	70° × 77°	450m
Solid state	Aeva	Aeries II	64	120° × 19.2°	150m

changes. Similarly, Boreas (Burnett et al. 2023) meets the conditions necessary for intra and inter-session place recognition. However, each sequences from both Boreas and the Ford Multi-AV dataset consists of similar paths, which reduces the complexity in inter-session place recognition. Additionally, Boreas also acquired data from a single LiDAR system. The Complex Urban Dataset (Jeong et al. 2019) and UrbanNav Dataset (Hsu et al. 2021), both situated within urban environments, lean more towards intra-session place recognition, offering limited avenues for inter-session recognition. The Wild Places (Knights et al. 2023) stands apart by ensuring both intra-session and inter-session place recognition, factoring in temporal variations. Yet, its focus remains on unstructured terrains and employs a single spinning LiDAR. Unlike the previous dataset, the Pohang Canal dataset (Chung et al. 2023) utilizes multiple LiDARs. However, inter-session place recognition is absent, and the trajectory of all sessions has an identical path. The NTU VIRAL dataset (Nguyen et al. 2022) also exploits multiple LiDARs; however, it leans more towards UAV localization, overshadowing the place recognition.

Many of aforementioned datasets primarily rely on spinning LiDARs. More recent datasets, such as Tiers (Qingqing et al. 2022), Hilti 2023 (Helmberger et al. 2022), and City (Jung et al. 2023) dataset, have begun to incorporate heterogeneous LiDARs. The Tiers and Hilti 2023 datasets feature short-term indoor and outdoor data collection using carlike vehicles and handheld systems. Similarly, the City dataset captures urban areas using a vehicle-based system. Although these datasets employ heterogeneous LiDARs, their primary focus is on SLAM. As a result, they tend to have relatively short paths, which means that revisits are either minimal or non-existent in sequences, rendering intra-session place recognition unfeasible. Additionally, the lack of overlap in their sequences means these datasets are unsuitable for validating inter-session place recognition.

The HeLiPR dataset distinguishes itself from others by showcasing a diverse LiDARs, encompassing the OS2-128, VLP-16, Livox Avia, and Aeva Aeries II, each with unique attributes. These sensors capture data channels such as NIR, reflectivity, and radial velocity, ushering in new avenues for inventive place recognition. Significantly,

**Figure 2.** Sensors coordinate information between sensors. (a) and (b) represent the transformation with the xy-plane and z-axis. The inter-sensor transformation after the extrinsic calibration can be found in the `Calibration` folder.

HeLiPR dataset captures each sequences over a month, supplying a rich environments which in turn supports both intra-session and inter-session place recognition. Furthermore, the HeLiPR dataset trajectories resonate with sequences derived from MulRan, thus promoting research in heterogeneous LiDAR place recognition and offering an extended temporal perspective. Conclusively, every sequence in HeLiPR illustrates a vast environment with variations.

3 System Overview

3.1 System Configuration

Our system comprises four distinct LiDARs, as depicted in Figure. 2 and Table. 2. The spinning OS2-128 LiDAR is mounted at the center of the system, elevated to allow dense scanning without any occlusion. This LiDAR offers additional channels such as reflectivity and NIR, furnishing geometric and textural data about the surrounding environment. In contrast, the spinning LiDAR, VLP-16, experiences particular occlusion because of its proximity to the front box and surrounding sensors. Also, due to inherent hardware constraints, it casts a significantly smaller ray than the OS2-128, enabling only a peripheral scan of its surroundings. The remaining LiDARs, Livox Avia and Aeva Aeries II are oriented to scan the front view

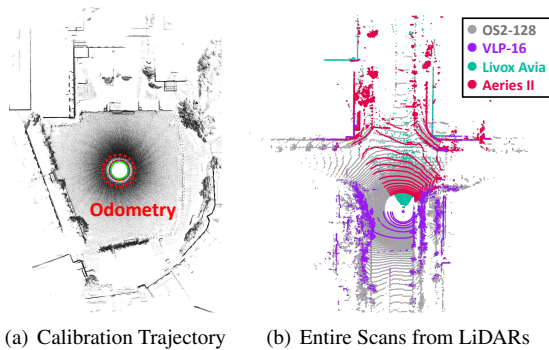


Figure 3. (a) Extrinsic calibration trajectory: A circular path used for map construction and calibration purposes. (b) Post-calibration LiDAR alignment: A sky plot view illustrating the overlap of contours between individual LiDAR scans.

of the vehicle, and each presents unique limitations. In the case of the Avia, its unconventional scanning patterns deviate from traditional spinning LiDARs; thus, direct comparison with them is challenging. However, Avia can construct dense maps with accumulating non-repetitive scans based on the relative transformation between scans. The Aeries II also presents a narrow horizontal FOV. There is an advantage of detecting radial velocities of points; however, it introduces noise into range measurements. This combination of LiDARs, with their unique scanning patterns, allows for an intriguing exploration in place recognition, including dealing with occlusion scenarios and contrasting low versus high resolution. Furthermore, leveraging the individual channels of these LiDARs could significantly enhance place recognition in environments characterized by substantial dynamics or rich textures. All of the LiDARs operate at a frequency of 10Hz.

In addition to the LiDARs, our system incorporates two types of inertial sensors, the inertial measurement unit (IMU) and the inertial navigation system (INS). These devices provide a means to determine the temporal and spatial relationships within the asynchronous LiDAR system. We employ the Xsens MTi-300, which measures inertial units at 100 Hz. We use the SPAN-CPT7 coupled with a dual VEXXIS GNSS-501 antenna to establish a baseline for the vehicle system. All baselines are achieved at a frequency of 50Hz using RTK GPS and INS. Due to each sensor acquiring measurements in its coordinate system, an extrinsic calibration process is necessary to integrate all the data into a standard coordinate system. This ensures consistency and accuracy across various measurements.

3.2 Sensor Calibration

We employ symbols to represent the coordinate systems for simplicity: L corresponds to the LiDAR, N signifies INS, I is used for IMU, and W indicates the world system.

3.2.1 Multiple LiDAR Extrinsic Calibration To calculate the extrinsic calibration between LiDARs, we utilize the existing calibration method (Liu et al. 2022). In this method, the trajectories from each LiDAR are obtained, and they are updated through batch optimization with scans from each LiDAR. After that, based on the updated trajectories and the initial extrinsic calibration parameters, batch optimization with multiple LiDARs is re-performed to calculate an accurate extrinsic calibration. To implement this method

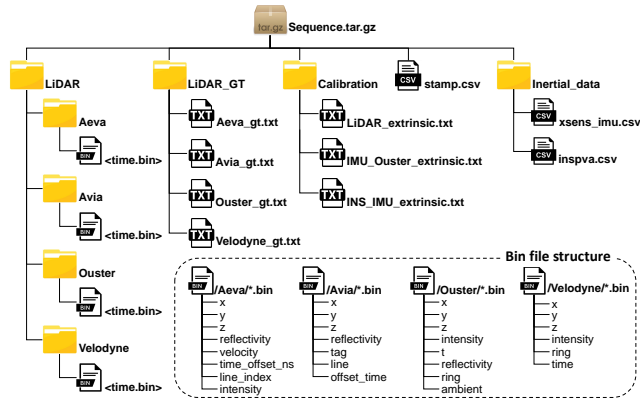
properly, a specified procedure is followed. The initial step involves moving the system a minimum distance to ensure trajectory accuracy. A complete 360-degree rotation follows this to facilitate the capture of loop closure for narrow FOV LiDARs. In the case of vehicles, given their inability to rotate in place, the system proceeded with a circular trajectory as shown in Figure. 3(a). Furthermore, considering the potential distortion of LiDAR that might occur during motion, we stop the movement for 10 seconds during a motion, and acquire a total of 30 scans with stationary. Lastly, considering the sparsity of a single scan from the Livox Avia, LiDAR scans are accumulated in a stationary condition. The initial extrinsic calibration is established using the CAD model. Additionally, the odometry for each LiDAR is obtained using Direct LiDAR Odometry (Chen et al. 2022). As depicted in Figure 3(b), it is clear that all the LiDARs are accurately aligned due to the precise extrinsic calibration.

3.2.2 IMU-LiDAR Extrinsic Calibration The extrinsic calibration between the IMU and the LiDAR commences with the CAD model serving as the initial estimation. The extrinsic calibration of the IMU-LiDAR (\mathbf{T}_I^L) is subsequently computed using LiDAR-Inertial Odometry (Xu et al. 2022a). It is updated while transforming the LiDAR scan to IMU coordinates and calculating the point-to-plane distance relative to the global map. However, achieving 6-DOF motion with a vehicle can prove challenging, which may adversely impact the accuracy of the extrinsic calibration between them. To mitigate this issue, the extrinsic calibration is updated with a minimal covariance, ensuring no significant deviation from the initial estimation. The entire process is executed based on the Roundabout01 sequence, leading to the calculation of extrinsic calibration between the OS2-128 and the IMU. The reason for selecting these two sensors is that they are positioned colinearly, resulting in an almost zero distance between one axis. Additionally, as the two sensors share the same axis, the initial estimate of these parameters remains the most accurate among all the LiDARs.

3.2.3 INS-IMU Extrinsic Calibration The extrinsic calibration between the INS and IMU is conducted using MA-LIO (Jung et al. 2023). This method is particularly effective for asynchronous LiDARs. As the trajectory from MA-LIO is aligned to the IMU coordinate system, the subsequent hand-eye calibration between the INS and IMU can be executed. Specifically, the relative transformation, or $\Delta\mathbf{T}^N$, between \mathbf{T}^N at two distinct timestamps t_i^N and t_j^N is determined. Similarly, the relative transformation, $\Delta\mathbf{T}^I$, between \mathbf{T}^I at timestamps t_i^I and t_j^I is ascertained. Considering the non-coincident time, t^N and t^I , we synchronize the acquisition time across both sensors to minimize time discrepancies. Then, the extrinsic calibration between the INS and IMU is achieved via the equation $\Delta\mathbf{T}^N\mathbf{T}_N^I = \mathbf{T}_N^I\Delta\mathbf{T}^I$. We employ 15000 transformations from the Roundabout01 sequence to carry out the calibration, with the maximum time difference registering at approximately 1ms. Moreover, it is worth noting that the fidelity of hand-eye calibration is inherently reliant on the precision of the MA-LIO. As such, we employ the CAD model specifically for the z-axis translation, which is most susceptible to errors in LIO. For all other components, we use the results from the hand-eye calibration.

Table 3. The Description for Each Sequence.

Sequence Name	Challenges	Sequence Index											
		01			02			03			04		
		Date	Duration	Distance	Date	Duration	Distance	Date	Duration	Distance	Date	Duration	Distance
Roundabout Town	Various rotation variations FOV issue in narrow areas	2023-07-16	2730s	9040m	2023-08-01	2085s	7447m	2023-08-13	2515s	9262m	-	-	-
		2023-07-18	2414s	7832m	2023-07-31	2689s	8203m	2023-08-14	2528s	8903m	-	-	-
Bridge	Similar scenes and dynamic objects	2023-07-17	2144s	23056m	2023-07-31	2562s	14615m	2023-08-14	2009s	19400m	2023-08-21	3033s	22958 m

**Figure 4.** File structure of the HeLiPR dataset, illustrating the organization of LiDAR scans, ground truths, calibration, and inertial sensor measurements for each sequence

4 Description of HeLiPR Dataset

4.1 Data Format

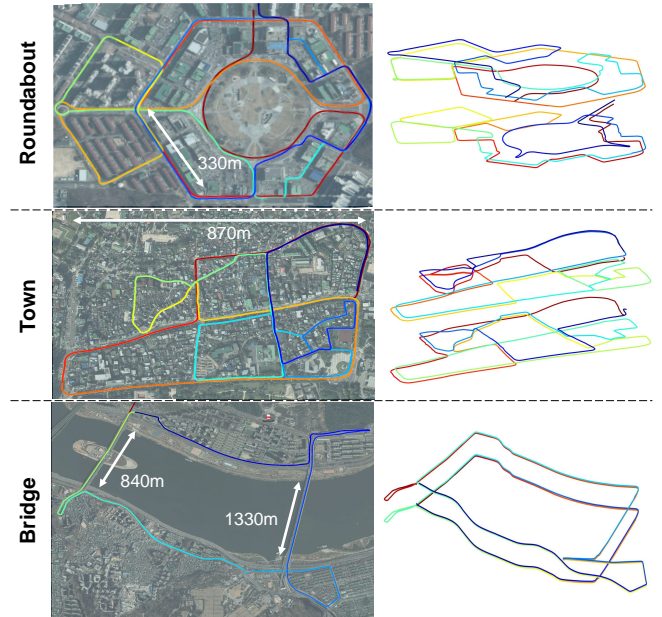
We offer sensor-specific data as individual files in diverse formats to optimize dataset management and facilitate access to each file and frame. Furthermore, we supply a file player based on Robot Operating System (ROS), tasked with reading and publishing these files into ROS topics, ensuring seamless accessibility for pre-existing place recognition and tasks like SLAM. The file structure of the HeLiPR dataset is delineated in Figure 4. The acquisition time of all measurements is stored in `stamp.csv`, and detailed descriptions of the data are presented subsequently.

4.1.1 Multiple LiDARs Data Individual LiDAR scans are stored as binary files in the `LiDAR/Sensor_name`. These files, identified as `<time.bin>`, encompass common channels such as (x, y, z) , time offset, and ring (or line) index. We illustrate the array of unique channels for each LiDAR and the order of their storage in Figure 4.

4.1.2 INS Data All INS data are stored in the `inspva.csv`. This file includes time, latitude, longitude, height, north_velocity, east_velocity, up_velocity, roll, pitch, azimuth, and data_status, organized in this order. Each value adheres to the East-North-Up (ENU) coordinate system, with the azimuth being determined by a left-handed rotation around the z-axis, in degrees, and clockwise from north.

4.1.3 IMU Data The complete set of IMU data is contained within the `xsens_imu.csv` file. Sequentially, this file encompasses time, quaternion (x, y, z, w) , Euler angles (x, y, z) , gyroscope (x, y, z) , acceleration (x, y, z) , and magnetic field (x, y, z) .

4.1.4 Calibration and Ground truth Data The results of extrinsic calibration are saved in the `Calibration`. Additionally, we derive the individual LiDAR ground truth based on INS, LiDAR acquisition time and calibration parameters. Within the `LiDAR_GT`, the ground truth for each LiDAR is recorded, incorporating scan time, position

**Figure 5.** INS-based trajectories for sequences 01, 02, and 03. The left shows trajectories on aerial images for 01, while the right visualizes 02 (bottom) and 03 (top) with a color gradient. Notably, red indicates the start point, while blue designates the end point.

(x, y, z) , and quaternion (x, y, z, w) . The procedure for generating this file is discussed in §4.3.

4.2 Sequence Explanation

In the HeLiPR dataset, we present three distinct places of the dataset, namely Roundabout, Town, and Bridge. Furthermore, these places are meticulously acquired through three repetitions denoted as 01–03, with a two-week interval between each acquisition. The deliberate interval introduces temporal changes to enable inter-session place recognition. It allows for spatial variations, such as lane changes or reversing directions, when capturing data at the same location but on different paths. Detailed information, including acquisition time, duration, and distance, can be found in the Table 3. Each sequences showcases unique environmental characteristics and introduces novel challenges in inter-LiDAR place recognition. We focused on enhancing both intra-session and inter-session loop closure candidates, with the primary objective of generating an abundant set of queries for place recognition. The trajectory of all sequences and their characteristics are represented in Figure 5 and Figure 6.

(i) Roundabout 01–03: Roundabout stands out as the most formal environment for place recognition among all the sequences. High buildings and wide roads enrich the dataset with abundant features that aid in place recognition. As its name suggests, it consists of three roundabouts: one large and two of a comparatively smaller size. The presence of a large roundabout and an outer hexagon design ensures

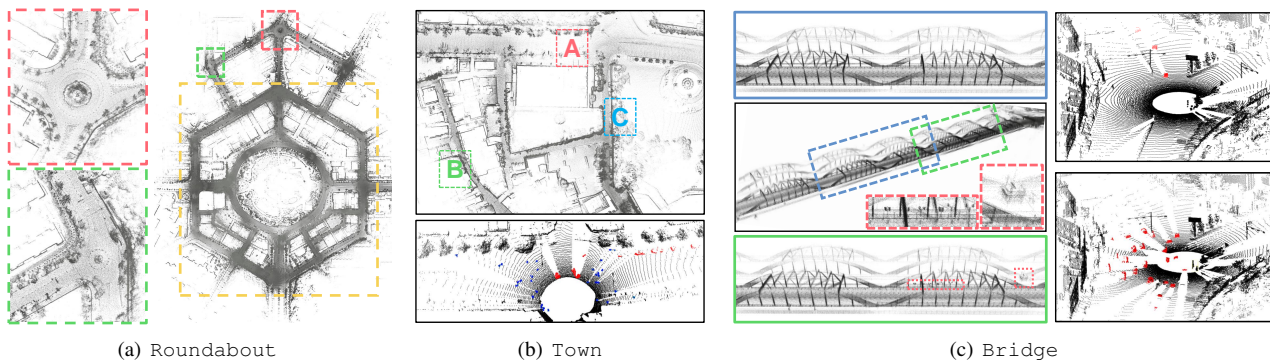


Figure 6. Characteristics of sequences. (a) Roundabout with three distinct roundabouts, each highlighted by a colored box. (b) Town showcasing a mix of narrow alleys and wider boulevards with width indications for areas A, B, and C, which are measured approximately 15m, 3m and 5m in width. Dynamic entities, such as pedestrians (blue) and vehicles (Red), are marked. (c) Bridge emphasizing the challenge of scene similarities within the sequence. The portions of the bridge highlighted in blue and green boxes appear remarkably similar but display subtle differences, as indicated in the red box. Additionally, the presence of dynamic objects (red) and variations in numbers between Bridge01 (upper) and Bridge02 (lower) pose quite challenges for place recognition.

easy revisiting of previously encountered locations. These roundabouts offer diverse rotational variations not typically encountered in regular road scenarios.

(ii) **Town01–03:** Town presents a wide road environment in the center of the route, facilitating efficient scanning of buildings and structures. This characteristic shares similarities with the Roundabout sequence. However, in Town, the buildings are relatively low compared to those observed in Roundabout, and narrow alleys are frequent. These alleys pose challenges in utilizing the wide sensing capabilities of LiDAR, creating a situation akin to indoor place recognition. These environment-related disparities add another layer of complexity to the place recognition, demanding sophisticated approaches to handle such spatial variations effectively.

(iii) **Bridge01–04:** Bridge consists of a total of 2 laps, covering two bridges with lengths of 1.3 km and 0.8 km, respectively. It should be noted that Bridge01 and Bridge04 differ from Bridge02 and Bridge03, with the former being driven using a reverse trajectory. This place introduces a significant challenge in place recognition due to the consecutive appearance of similar scenes in most areas. Additionally, numerous dynamic objects further complicate the recognition, particularly depending on the sequence index. Bridge02 and Bridge04 exhibit relatively slow speed distribution due to the presence of many dynamic objects. Notably, the Aeries II, which is a Frequency modulated continuous wave (FMCW) LiDAR, allows for measuring the radial velocity of a point, enabling the detection of certain dynamic objects. This capability opens up the potential for developing a novel place recognition based on this specific sequence and leveraging the unique features of the Aeries II.

4.3 Individual LiDAR Ground truth

For verification in place recognition, the positions between the query and the candidate must be determined, necessitating the precise positions of the LiDAR at each timestamp. Although all LiDARs capture the scans under the Coordinate Universal Time (UTC) facilitated by Precision Time Protocol (PTP), the individual acquisition times for each scan can vary. This discrepancy introduces complexity when attempting to ascertain the positions within their unique timestamp.

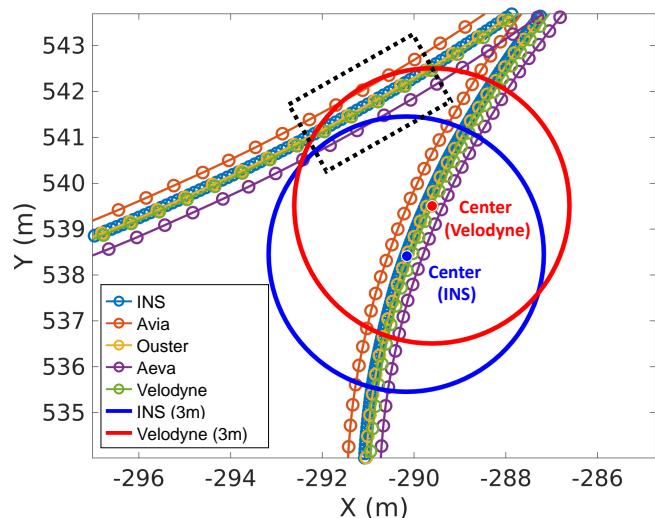


Figure 7. Partial individual ground truth for Roundabout01. Using individual ground truth with Velodyne as a reference, true positive place recognition candidates are observed for all LiDARs within a 3m radius of other paths (black box). However, exact matches with the INS location (within a 5ms discrepancy) are only found in Aeva.

As depicted in Figure. 7, each LiDAR exhibits distinct trajectories due to sensor placement and acquisition time variations. Leveraging these diverse trajectories in place recognition offers significant advantages over relying solely on ground truth from a single sensor. Notably, the spatial relationship between each sensor plays a crucial role. For instance, during revisits to previously encountered locations, specific LiDAR pairs might exhibit proximity, qualifying as true positives based on a predetermined threshold criterion. However, other LiDAR pairs may appear to be substantially distant from each other, potentially affecting the recognition accuracy. This issue indicates the significance of LiDAR spatial relationship and time delays in place recognition. Therefore, the ability to consider such differences can be an advantage when leveraging multiple LiDARs, and it would be more practical than utilizing a single ground truth. Furthermore, as LiDARs and INS are collected asynchronously, a lack of positional alignment arises, leading to potential discrepancies and inaccuracies in place recognition.

While INS operates at a frequency of 50Hz, five times faster than the LiDAR, relying solely on linear

Table 4. The Description for Additional Sequences.

Sequence Name	Sequence Index					
	04			05		
	Time	Duration	Distance	Time	Duration	Distance
KAIST	Night	1261s	6348m	Daytime	1248s	6878m
DCC	Night	786s	5506m	Daytime	1081s	5309m
Riverside	Night	612s	6523m	Daytime	855s	6394m

approximation can be imprecise. To address this issue, we initially establish INS position that aligns with the timestamp of each LiDAR using B-spline interpolation (Mueggler et al. 2018). Given that the k^{th} scan of a specific LiDAR, denoted as L_k , is acquired at time t_k , this position, $\mathbf{T}_W^N = (\mathbf{R}_W^N, \mathbf{t}_W^N)$ can be determined by leveraging four nearby INS measurements as control points. Nevertheless, our primary interest lies in determining the location of $\mathbf{T}_W^L = (\mathbf{R}_W^L, \mathbf{t}_W^L)$ in the world coordinates of L . It can be calculated as the multiplication with \mathbf{T}_W^N , IMU-LiDAR (\mathbf{T}_I^L) and INS-IMU (\mathbf{T}_N^I) extrinsic calibration. To enhance user convenience, we standardize \mathbf{T}_W^L using the Universal Transverse Mercator (UTM) coordinate system, opting not to employ latitude or longitude. This decision simplifies plotting processes, and these coordinates streamline the direct comparison of trajectories with each other and with the MulRan dataset.

In summary, embracing the individual trajectories of multiple LiDARs allows for a more comprehensive evaluation of spatial and temporal variations, contributing to improved place recognition outcomes.

4.4 HeLiPR Dataset: Long-Term Place Recognition in Tandem with MulRan

The HeLiPR dataset not only encompasses the sequences of Roundabout, Town, and Bridge, but also integrates sequences from the MulRan dataset, including KAIST, DCC, and Riversside, catering to long-term place recognition. Contrary to the MulRan data captured with OS1-64, the HeLiPR dataset employs the aforementioned LiDARs. This introduces the potential for heterogeneous LiDAR place recognition. Furthermore, with a temporal variance spanning approximately four years, offering a novel challenge.

Each sequence in the HeLiPR dataset is composed of 04 and 05. The 04 sequence was captured during the night and is characterized by an almost complete absence of dynamic objects. In contrast, the 05 sequence, captured during the day, features a diverse dynamic objects, mirroring the existing MulRan sequences. A comprehensive overview of each sequence can be found in Table 4 and Figure 8. Thanks to the GPS and INS, the trajectories of KAIST03 from MulRan and KAIST04-05 align seamlessly even though these were captured at distinct times, enabling place recognition. As observed in Figure 8, certain areas undergo partial modifications. These areas, both changed and preserved, are valuable not just for place recognition but also for change detection and map maintenance.

5 Benchmark Results with HeLiPR Dataset

In this section, we present an exhaustive analysis of the current state-of-the-art place recognition using the HeLiPR dataset. The comprehensive evaluation aims not only to identify the present capabilities of state-of-the-art place recognition but also to emphasize the inherent

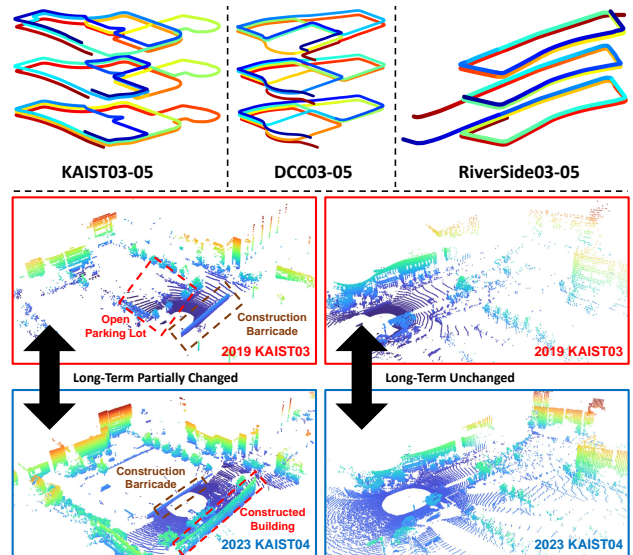


Figure 8. (Top row) Trajectories derived from GPS and INS measurements. Similar to Figure 5, three trajectories for each location are plotted. (Bottom row) A comparison of the environmental changes between KAIST03 and KAIST04.

need and importance of having datasets like HeLiPR to advance the field further. To assess the performance of the methodologies, which include Scan Context (SC) (Kim et al. 2021), STD (Yuan et al. 2023), RING++ (Xu et al. 2022b) and LoGG3D-Net (Vidanapathirana et al. 2022), we employ two evaluation metrics: the Precision-Recall curve (PR-curve) and the Area Under the Curve (AUC) score.

Precision-Recall Curve (PR-Curve): This curve is an illustrative representation of a precision versus its recall. It provides a comprehensive visualization of the performance across different threshold levels. Mathematically, it can be expressed by the following equations:

$$\text{Precision} = \frac{\text{TP}}{\text{TP} + \text{FP}}, \quad \text{Recall} = \frac{\text{TP}}{\text{TP} + \text{FN}} \quad (1)$$

where TP denotes true positives, FP represents false positives, and FN signifies false negatives.

Area Under the Curve (AUC): This metric evaluates the overall performance of a place recognition. The AUC score provides a singular scalar value that summarizes the entire PR-curve. A perfect recognition method would achieve an AUC of 1.0, indicating flawless recognition, while a score closer to 0.5 might indicate a method performing no better than random guessing.

For the evaluation, the methodology entails sampling query scans at 10m intervals and target scans at 5m intervals. A successful place recognition is defined by the identification of a candidate within a 7.5m, termed as a true positive. All scans have been undistorted and are configured with a maximum range of 100m for descriptor extraction. For methods other than STD, only the scans from Livox Avia are grouped into sets of 20, due to its sparse point distribution. However, when evaluating STD, similar with the original research, we accumulate 20 scans for every type of LiDAR. This approach differentiates it from other methods that typically use a single scan. LoGG3D-Net mines quadruplet for every query point cloud that exists in each sequence. Since our work deals with place recognition between various LiDARs, we viewed data

Table 5. AUC score for inter-session place recognition

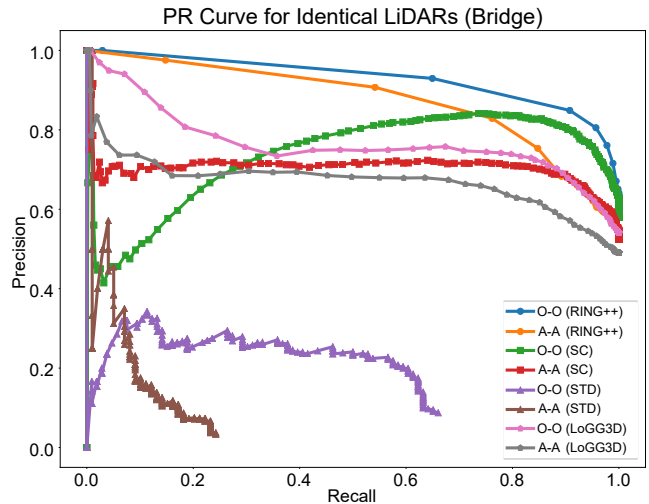
Sequences	Method	Identical LiDARs		Heterogeneous LiDARs		
		O-O	A-A	O-V	O-A	O-L
Roundabout01-03	SC	0.982	0.890	0.690	0.045	0.102
	STD	0.171	0.044	0.000	0.010	0.002
	RING++	0.975	0.934	0.111	0.003	0.005
	LoGG3D	0.826	0.748	0.558	0.619	0.263
Town01-03	SC	0.985	0.908	0.796	0.212	0.396
	STD	0.202	0.022	0.000	0.001	0.000
	RING++	0.972	0.981	0.248	0.004	0.003
	LoGG3D	0.865	0.766	0.507	0.603	0.371
Bridge02-03	SC	0.732	0.705	0.400	0.368	0.241
	STD	0.160	0.056	0.000	0.001	0.000
	RING++	0.938	0.878	0.054	0.003	0.003
	LoGG3D	0.764	0.670	0.426	0.548	0.317

- Symbol denotes LiDARs. (O: Ouster, A: Aeva, L: Livox, V: Velodyne) acquired at the same time and space(ex. DCC05/Ouster, DCC05/Aeva, DCC05/Ouster, DCC05/Livox and DCC05/Velodyne) as single super sequence(ex. DCC05). For training, 6 super sequences (DCC04-05, KAIST04-05, and Riverside04-05) are utilized. We followed the training schemes and parameters of the original paper: we only replaced positive sampling distance to 7.5m and the number of negatives to 8.

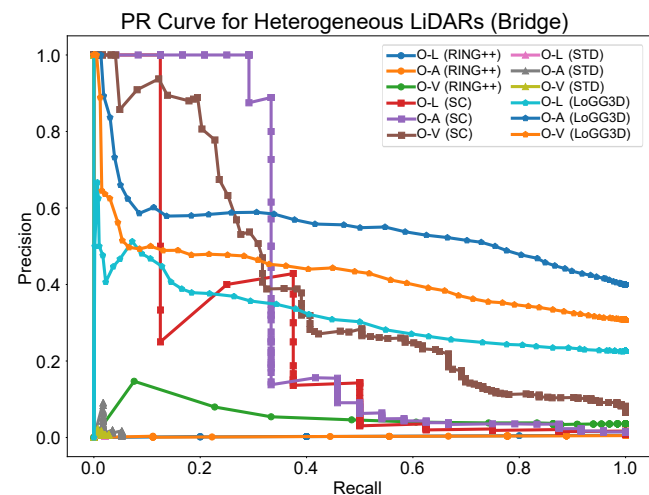
We evaluate each method using three inter-session pairs: Roundabout01-03, Town01-03, and Bridge02-03. Using Ouster as the reference database, we employ various LiDARs as queries to identify the corresponding Ouster candidates. To assess the influence of FOV, we also perform evaluations using the same LiDAR type. As detailed in Table. 5, we assess the four methods across three environments using five LiDAR pairings. This experimental configuration underscores the expansive scenarios of place recognition that the HeLiPR dataset can facilitate.

From Figure. 9 and Table. 5, we can discern several insights about the performance of place recognition. Most methods tend to exhibit superior performance in Roundabout and Town compared to Bridge, likely due to the distribution of structures and inherent challenges highlighted in Figure. 6. Furthermore, spinning LiDAR generally achieves better results with a higher AUC score than solid-state LiDAR. This is anticipated given that spinning LiDARs boast a broader FOV. This expansive FOV equips them to adeptly handle place recognition from varied directions, including in scenarios like reversing or navigating intersections. Unlike the other methods, STD cannot handle the inter-session place recognition even exploiting accumulated scans. For STD, a triangle descriptor is chosen based on three vertices. However, the inability to consistently select a vertices, owing to changes in static objects like parked cars and the presence of dynamic objects, appears to be a primary factor in its performance degradation. LoGG3D-Net exhibits slightly lower performance with temporal discrepancies. This may be mainly due to the fact that each training quadruplet were mined from each super sequences, thereby missing pairs with long-term variance.

In the case of the heterogeneous LiDAR place recognition, a performance dip is observed. Most other heterogeneous LiDAR configurations largely underperform in model-based place recognition, such as Scan Context, STD, and RING++. Notably, only the Scan Context maintains a normal performance across various environments with Velodyne. This could be ascribed to the similarities between Velodyne and Ouster, given that both are spinning LiDARs with



(a) PR-Curve for Identical LiDAR (Bridge)



(b) PR-Curve for Heterogeneous LiDAR (Bridge)

Figure 9. PR-Curve of inter-session place recognition between Bridge02 and Bridge03. (a) depicts the results when identical LiDAR systems are compared, illustrating the performance when different types of LiDARs each match with an identical LiDAR. (b) showcases the outcomes when heterogeneous LiDARs are used.

analogous FOV values, leading to similar maximum z-values. Similarly, Scan Context demonstrates superior results compared to other methods for heterogeneous LiDAR place recognition, particularly in the Town. For LoGG3D-Net, Aeva shows the best performance among others. Since the number of vertical channels between Ouster and Aeva are similar, it could empower the better local feature aggregation ability for local consistency loss between point clouds. However, when considering other sequences and alternative methods, the challenge of effectively handling heterogeneous LiDAR-based place recognition remains evident, with most approaches falling short of achieving satisfactory results. This analysis serves to underline the necessity for more focused research in the realm of heterogeneous LiDAR place recognition and stands testament to the pivotal role the HeLiPR dataset can play in spurring such investigations.

6 Conclusion

The HeLiPR dataset stands as a comprehensive resource that has been meticulously curated to showcase the remaining

challenges of place recognition. It encompasses a broad spectrum of data from varied environments, including Roundabout, Town, and Bridge. One of the unique attributes of this dataset is its collection method; by introducing intentional time intervals and capturing data along diverse paths, we are ensuring the data reflects real-world spatial-temporal challenges. This not only mimics the dynamic nature of real-world scenarios but also enhances the application in localization and place recognition tasks. Additionally, for long-term place recognition, the HeLiPR dataset overlaps with the MulRan dataset, presenting novel challenges in the realm of place recognition. With these features, the HeLiPR dataset is poised to become a valuable resource for improving place recognition and robotics applications, promoting advancements in the field.

Acknowledgements

This research was conducted with the support of the "National R&D Project for Smart Construction Technology (23SMIP-A158708-04)" funded by the Korea Agency for Infrastructure Technology Advancement under the Ministry of Land, Infrastructure and Transport, and managed by the Korea Expressway Corporation.

References

- Agarwal S, Vora A, Pandey G, Williams W, Kourous H and McBride J (2020) Ford multi-av seasonal dataset. *Intl. J. of Robot. Research* 39(12): 1367–1376.
- Arandjelovic R, Gronat P, Torii A, Pajdla T and Sivic J (2016) Netvlad: Cnn architecture for weakly supervised place recognition. In: *Proc. IEEE Conf. on Comput. Vision and Pattern Recog.* pp. 5297–5307.
- Barnes D, Gadd M, Murcutt P, Newman P and Posner I (2020) The oxford radar robotcar dataset: A radar extension to the oxford robotcar dataset. In: *Proc. IEEE Intl. Conf. on Robot. and Automat.*
- Burnett K, Yoon DJ, Wu Y, Li AZ, Zhang H, Lu S, Qian J, Tseng WK, Lambert A, Leung KY, Schoellig AP and Barfoot TD (2023) Boreas: A multi-season autonomous driving dataset. *Intl. J. of Robot. Research* 42(1-2): 33–42.
- Chen K, Lopez BT, Agha-mohammadi Aa and Mehta A (2022) Direct lidar odometry: Fast localization with dense point clouds. *IEEE Robot. and Automat. Lett.* 7(2): 2000–2007.
- Chen X, Läbe T, Milioto A, Röhling T, Vysotska O, Haag A, Behley J and Stachniss C (2020) OverlapNet: Loop Closing for LiDAR-based SLAM. In: *Proc. Robot.: Science & Sys. Conf.*
- Chung D, Kim J, Lee C and Kim J (2023) Pohang canal dataset: A multimodal maritime dataset for autonomous navigation in restricted waters. *Intl. J. of Robot. Research* 0(0): 02783649231191145.
- Geiger A, Lenz P and Urtasun R (2012) Are we ready for autonomous driving? the kitti vision benchmark suite. In: *Proc. IEEE Conf. on Comput. Vision and Pattern Recog.*
- Helmberger M, Morin K, Berner B, Kumar N, Cioffi G and Scaramuzza D (2022) The hilti slam challenge dataset. *IEEE Robot. and Automat. Lett.* 7(3): 7518–7525.
- Hsu L, Kubo N, Wen W, Chen W, Liu Z, Suzuki T and Meguro J (2021) Urbannav: An open-sourced multisensory dataset for benchmarking positioning algorithms designed for urban areas. In: *ION GNSS+*. pp. 226–256.
- Jeong J, Cho Y, Shin YS, Roh H and Kim A (2019) Complex urban dataset with multi-level sensors from highly diverse urban environments. *Intl. J. of Robot. Research* 38(6): 642–657.
- Jung M, Jung S and Kim A (2023) Asynchronous multiple lidar-inertial odometry using point-wise inter-lidar uncertainty propagation. *IEEE Robot. and Automat. Lett.*
- Kim G, Choi S and Kim A (2021) Scan context++: Structural place recognition robust to rotation and lateral variations in urban environments. *IEEE Trans. Robot.* 38(3): 1856–1874.
- Kim G, Park YS, Cho Y, Jeong J and Kim A (2020) Mulran: Multimodal range dataset for urban place recognition. In: *Proc. IEEE Intl. Conf. on Robot. and Automat.* pp. 6246–6253.
- Knights J, Vidanapathirana K, Ramezani M, Sridharan S, Fookes C and Moghadam P (2023) Wild-places: A large-scale dataset for lidar place recognition in unstructured natural environments. In: *Proc. IEEE Intl. Conf. on Robot. and Automat.*
- Lee AJ and Kim A (2021) Eventvlad: Visual place recognition with reconstructed edges from event cameras. In: *Proc. IEEE/RSJ Intl. Conf. on Intell. Robots and Sys.* pp. 2247–2252.
- Liu X, Yuan C and Zhang F (2022) Targetless extrinsic calibration of multiple small fov lidars and cameras using adaptive voxelization. *IEEE Trans. Instrum. and Meas.* 71: 1–12.
- Luo L, Cao SY, Han B, Shen HL and Li J (2021) Bvmatch: Lidar-based place recognition using bird’s-eye view images. *IEEE Robot. and Automat. Lett.* 6(3): 6076–6083.
- Mueggler E, Gallego G, Rebecq H and Scaramuzza D (2018) Continuous-time visual-inertial odometry for event cameras. *IEEE Trans. Robot.* 34(6): 1425–1440.
- Nguyen TM, Yuan S, Cao M, Lyu Y, Nguyen TH and Xie L (2022) Ntu viral: A visual-inertial-ranging-lidar dataset, from an aerial vehicle viewpoint. *Intl. J. of Robot. Research* 41(3): 270–280.
- Qingqing L, Xianjia Y, Queraltá JP and Westerlund T (2022) Multi-modal lidar dataset for benchmarking general-purpose localization and mapping algorithms. In: *Proc. IEEE/RSJ Intl. Conf. on Intell. Robots and Sys.* pp. 3837–3844.
- Shan T, Englot B, Duarte F, Ratti C and Rus D (2021) Robust place recognition using an imaging lidar. In: *Proc. IEEE Intl. Conf. on Robot. and Automat.* pp. 5469–5475.
- Vidanapathirana K, Ramezani M, Moghadam P, Sridharan S and Fookes C (2022) Logg3d-net: Locally guided global descriptor learning for 3d place recognition. In: *Proc. IEEE Intl. Conf. on Robot. and Automat.* pp. 2215–2221.
- Wang H, Wang C and Xie L (2020) Intensity scan context: Coding intensity and geometry relations for loop closure detection. In: *Proc. IEEE Intl. Conf. on Robot. and Automat.* pp. 2095–2101.
- Xu W, Cai Y, He D, Lin J and Zhang F (2022a) Fast-lid2: Fast direct lidar-inertial odometry. *IEEE Trans. Robot.* 38(4): 2053–2073.
- Xu X, Lu S, Wu J, Lu H, Zhu Q, Liao Y, Xiong R and Wang Y (2022b) Ring++: Roto-translation invariant gram for global localization on a sparse scan map. *arXiv preprint arXiv:2210.05984*.
- Yuan C, Lin J, Zou Z, Hong X and Zhang F (2023) Std: Stable triangle descriptor for 3d place recognition. In: *C-ICRA*.
- Zhang Y, Jin R and Zhou ZH (2010) Understanding bag-of-words model: a statistical framework. *International journal of machine learning and cybernetics* 1: 43–52.